ACKNOWLEDGMENTS

This work is supported by the Key Project of National Natural Science Fund (no. 90207004) and the National Natural Science Fund (no. 60306005), a collaborative project between Peking University and Intel Corporation. The authors thank the Institute of Microelectronics of Chinese Academy of Sciences (IMECAS) for measurement support.

REFERENCES

1. R.J. Fontana, Recent system applications of short-pulse ultra-wideband (UWB) technology, IEEE Trans MTT 52 (2004), 2087–2104.
2. In the matter of Revision of Part 15 of the Commission's Rules Regarding Ultra-Wideband Transmission Systems ET Docket 98-153 First Report and Order; adopted: February 14, 2002; released: April 22, 2002, available at http://www.fcc.gov/Bureaus/Engineering_Technology/Orders/2002/fcc02048.pdf.
3. K. Mandke, H. Nam, I. Yerramneni, C. Zuniga, and T. Rappaport, The evolution of ultra-wideband radio for wireless personal area networks, High Freq Electron (2003), 22–32.
4. C.W. Kim, M.S. Kang, P.T. Anh, H.T. Kim, and S.G. Lee, An ultra-wideband CMOS low-noise amplifier for 3–5-GHz UWB systems, IEEE J Solid-State Circ 40 (2005), 544–547.
5. K.H. Chen and C.K. Wang, A 3.1–10.6-GHz CMOS cascaded two-stage distributed amplifier for ultra-wideband application, IEEE Asia-Pacific Conf Adv Syst Integrated Circ (AP-ASIC), 2004, pp. 296–299.
6. R. Hu, An 8–20-GHz wideband LNA design and the analysis of its input matching mechanism, IEEE Microwave Wireless Compon Lett 14 (2004), 528–530.
7. A. Bevilacqua and A.M. Niknejad, An ultra-wideband CMOS LNA for 3.1 to 10.6 GHz wireless receivers, IEEE Int Solid-State Circ Conf (ISSCC'04), 2004, pp. 382–383.
8. A. Ismail and A. Abidi, A 3- to 10-GHz LNA using a wideband LC-ladder matching network, Dig Tech Papers IEEE Int Solid-State Circ Conf (ISSCC'04), 2004, pp. 384–385.
9. R.C. Liu, K.L. Deng, and H. Wang, A 0.6–22-GHz broadband CMOS distributed amplifier, Proc IEEE Radio Freq Integrated Circ (RFIC) Symp, Philadelphia, PA, 2003, pp. 103–106.
10. S. Andersson, C. Svensson, and O. Drugge, Wideband LNA for a multistandard wireless receiver in 0.18 μm CMOS, in Proc. 2003 Eur Solid-State Circ Conf (ESSCIRC'03), 2003, pp. 655–658.

A NOVEL HIGH-ORDER TIME-DOMAIN SCHEME FOR THREE-DIMENSIONAL MAXWELL'S EQUATIONS

Zhi-Xiang Huang, Wei Sha, Xian-Liang Wu, and Ming-Sheng Chen
Key Laboratory of Intelligent Computing & Signal Processing
Anhui University
Ministry of Education
Hefei 230039, P.R. China

Received 24 November 2005

ABSTRACT: *A novel high-order time-domain scheme with a four-stage optimized symplectic integrator propagator is presented for 3D electromagnetic scattering problems. The scheme is nondissipative and does not require more storage than the classical finite-difference time-domain (FDTD) method. The numerical results show the scheme has better stability and more efficiency than the classical FDTD method.* © 2006 Wiley Periodicals, Inc. Microwave Opt Technol Lett 48: 1123–1125, 2006; Published online in Wiley InterScience (www.interscience.wiley.com). DOI 10.1002/mop.21563

Key words: *high-order time-domain scheme; symplectic integrator propagator; finite-difference time-domain (FDTD)*

1. INTRODUCTION

As the most standard method, the classical finite-difference time-domain (FDTD) method, which is 2nd-order accurate both in space and time, has been thoroughly established and widely used in computational electromagnetics (CEM) up to the present [1–3]. Unfortunately, for electrically large domains and late-time analysis, the classical Yee method begins to show its limitations due to the accumulation of phase errors. One solution is to use high-order schemes. For example, in the work of Fang [4], a 4th-order central-difference approximation is proposed in conjugation with the Yee cell [1] and a modified 4th-order leapfrog integrator is employed. In deriving Fang's method, a 3rd-order correctional temporal derivative was introduced and then converted into 3rd-order spatial derivatives through repeated application of the Maxwell's equations. So the method is difficult to deal with perfectly matched layer (PML) absorbing boundary conditions [5] for simulating unbounded domains and in calculating the varying of the permittivity or permeability in inhomogeneous domains. Another solution is to make use of the explicit four-stage Runge–Kutta integrator to approximate the temporal derivatives together with a compact central-difference approximation with the Yee cell to the space derivatives in the Maxwell's equations [6]. It should be noted, however, that the method produces not only phase error, but also amplitude error. Moreover, it requires additional memory for temporary storage of data for the internal stages.

Symplectic methods include a variety of different time-discretization methods designed to preserve the global symplectic structure of the phase space for a Hamiltonian system. They show substantial benefits in numerical computation for a Hamiltonian system, especially in long-term simulations. Since the Maxwell's equations can be written as a system of an infinite-dimensional Hamiltonian system, the proper solution should be obtained using symplectic methods, which preserve the symplectic structure in the time direction. Recently, symplectic methods have been adopted for use in CEM. The advantages of symplectic methods have been verified in [7–12]. The application of symplectic integrator propagator for solving Maxwell's Equations was made in [7] to obtain a 4th-order symplectic FDTD method, and in [13] an optimized symplectic integrator propagator coefficients was presented. In this paper, we make use of the four-stage optimized propagator coefficients in [13] to discretize 3D Maxwell's equations in the time direction, and use a 4th-order difference operator to discretize the 1st-order space differential operators directly. The bistatic radar cross section (RCS) of a dielectric sphere are computed using the present scheme for the first time.

2. THE THEORY

Maxwell's equations in an isotropic and sourceless medium can be written in matrix form as

$$\frac{\partial}{\partial t}\begin{pmatrix}\mathbf{H}\\ \mathbf{E}\end{pmatrix} = (A+B)\begin{pmatrix}\mathbf{H}\\ \mathbf{E}\end{pmatrix}, \tag{1}$$

$$A = \begin{pmatrix} -\mu^{-1}\sigma^*\mathbf{I}_3 & -\mu^{-1}R \\ \{0\}_{3\times 3} & \{0\}_{3\times 3}\end{pmatrix}, \quad B = \begin{pmatrix} \{0\}_{3\times 3} & \{0\}_{3\times 3} \\ \varepsilon^{-1}R & -\varepsilon^{-1}\sigma\mathbf{I}_3\end{pmatrix}, \tag{2}$$

where μ and ε are the respective permeability and permittivity, σ and σ^* are the respective electric and magnetic conductivities, $\{0\}_{3\times 3}$ is the 3×3 null matrix, $\mathbf{I}_3$ is the 3×3 unit matrix, R is the 3×3 matrix representing the 3D curl operator.

Since the matrices A and B do not commute (that is, $AB \neq BA$). So in the time direction, after the temporal increment Δ_t, the symplectic integrator propagator can be adopted to approximate

$$\exp(\Delta_t(A + B)) = \prod_{l=1}^{m} \exp(D_l \Delta_t B)\exp(C_l \Delta_t A) + O(\Delta_t^{n+1}), \quad (3)$$

where C_l and D_l are constant coefficients of the propagator. In this paper, particularly, we use the four-stage optimized propagator coefficients in [13].

The propagators can be calculated as follows:

$$\exp(\Delta_t A) = \begin{pmatrix} \exp\left(\dfrac{\Delta_t \sigma^*}{\mu}\right)\mathbf{I}_3 & \dfrac{1 - \exp\left(\dfrac{\Delta_t \sigma^*}{\mu}\right)}{\sigma^*} R \\ \{0\}_{3\times3} & \mathbf{I}_3 \end{pmatrix}, \quad (4)$$

$$\exp(\Delta_t B) = \begin{pmatrix} \mathbf{I}_3 & \{0\}_{3\times3} \\ \dfrac{1 - \exp\left(-\dfrac{\Delta_t \sigma}{\varepsilon}\right)}{\sigma} R & \exp\left(-\dfrac{\Delta_t \sigma}{\varepsilon}\right)\mathbf{I}_3 \end{pmatrix}. \quad (5)$$

As for the space direction, we use Yee's cell [1] and a 4$^{\text{th}}$-order difference operator to discretize the 1$^{\text{st}}$-order space differential operators as

$$\left(\frac{\partial f}{\partial x}\right) \approx \frac{27(f_{i+1/2} - f_{i-1/2}) - f_{i-3/2} + f_{i-3/2}}{24\Delta_x}. \quad (6)$$

Thus, the proposed scheme is referred to as a novel high-order time-domain scheme.

In the sourceless and lossless space, as an example, the detailed expressions of the x component of the normalized $\bar{\mathbf{E}}$, that is, $\bar{\mathbf{E}} = \sqrt{\varepsilon_0/\mu_0}\,\mathbf{E}$, in the scheme can be derived as

$$\begin{aligned} \bar{E}_x^{n+l/4}\left(i+\frac{1}{2}, j, k\right) &= \bar{E}_x^{n+l/4}\left(i+\frac{1}{2}, j, k\right) + \frac{1}{\varepsilon_r} \times \left\{ Coef_1 \times \left[H_z^{n+(l-1)/4}\left(i+\frac{1}{2}, j+\frac{1}{2}, k\right) - H_z^{n+(l-1)/4}\left(i+\frac{1}{2}, j-\frac{1}{2}, k\right) \right.\right. \\ &\left. - H_y^{n+(l-1)/4}\left(i+\frac{1}{2}, j, k+\frac{1}{2}\right) + H_y^{n+(l-1)/4}\left(i+\frac{1}{2}, j, k-\frac{1}{2}\right) \right] + Coef_2 \times \left[H_z^{n+(l-1)/4}\left(i+\frac{1}{2}, j+\frac{3}{2}, k\right) - H_z^{n+(l-1)/4}\left(i+\frac{1}{2}, j-\frac{3}{2}, k\right) \right. \\ &\left.\left. - H_y^{n+(l-1)/4}\left(i+\frac{1}{2}, j, k+\frac{3}{2}\right) + H_y^{n+(l-1)/4}\left(1+\frac{1}{2}, j, k-\frac{3}{2}\right) \right]\right\}, \end{aligned} \quad (7)$$

$$Coef_1 = \frac{9}{8} D_l \times \text{CFL}, \quad (8)$$

$$Coef_2 = \frac{-1}{24} D_l \times \text{CFL}, \quad (9)$$

$$\text{CFL} = \frac{\Delta_t}{\Delta_s \cdot \sqrt{\mu_0 \varepsilon_0}}, \quad (10)$$

where $n + l/4$ is the l^{th} stage calculation after the n^{th} step, ε_r is the local relative permittivity at point $(i + 1/2, j, k)$, and $\varepsilon = \varepsilon_r \varepsilon_0$, CFL is the Courant–Friedrichs–Levy number, and Δ_t and Δ_s are the temporal and uniform spatial increment, respectively. In the following numerical examples, we use a similar technique to discretize a 1D incident field based on a 4$^{\text{th}}$-order approximation, and the total-field and scattered-field (TF-SF) formulation is revised according to the requirements of consistency between TF-SF boundaries. The high-order PML absorbing boundary condition is employed to solve unbounded electromagnetic scattering problems. In order to obtain the values of scattered fields on every cell's center, high-order cubic interpolation is adopted here, and high-order near-to-far-field transformation is implemented to obtain the bistatic RCS.

3. NUMERICAL RESULTS

Consider a dielectric sphere illuminated by a plane wave propagating in the z direction and **E**-polarized in the x direction. The frequency of the incident wave is 300 MHz. The sphere has a diameter of 1.0 m, relative permittivity $\varepsilon_r = 4$, and a conductivity of 0.3. The size of the cell is 5.0 cm. The total computational domain is $83 \times 83 \times 83$ cells, the total field occupies $34 \times 34 \times 34$ cells, and 10 PML layers are implemented. A Mie series is presented as an analytical solution. Figure 1 shows the bistatic RCS in the E-plane simulated within 1700 time steps. The results computed by our scheme and FDTD are in very good agreement with the analytical solution when CFL is 0.5. The global relative root-mean-squares RCS error is 0.2123 using our scheme, as compared to 0.2247 using the classical FDTD method. In Figure 2, the results calculated by the FDTD method fail to be consistent with the analytical solution where CFL = 0.8 and 1.0 ($>(1/\sqrt{3})$, the limit of CFL is classical FDTD method), while our scheme still complies with the analytical solution. Clearly, the results demonstrate that the present scheme has better stability compared with

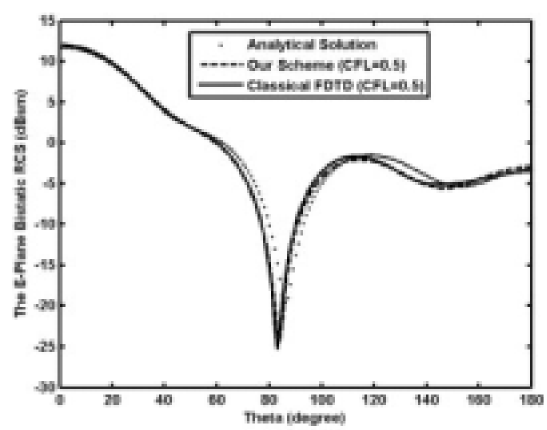

Figure 1 E-plane bistatic RCS of the dielectric sphere with CFL = 0.5

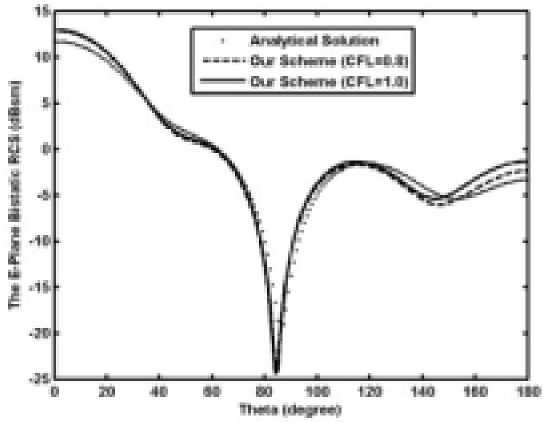

Figure 2 E-plane bistatic RCS of the dielectric sphere with different CFL number

the classical FDTD method and the error achieved by our scheme is smaller than that by the classical FDTD method.

4. CONCLUSION

A novel high-order time-domain scheme has been presented. The scheme was obtained by discretization of Maxwell's equations with a four-stage optimized symplectic integrator propagator in the time direction, and a 4^{th}-order difference operator in order to discretize the 1^{st}-order space differential operators directly. The scheme is nondissipative and does not require more storage than the classical FDTD method. Especially, the scheme has better stability and more efficiency than the classical FDTD method.

The major shortcoming of the scheme is that it consumes more CPU time than the classical FDTD method when the same cell size is used. An effective parallel algorithm is an open question for further study.

ACKNOWLEDGMENTS

This work was partially supported by the National Natural Science Foundation of China (No. 60371041).

REFERENCES

1. K.S. Yee, Numerical solution of initial boundary value problems involving Maxwell's equations in isotropic media, IEEE Trans Antennas Propagat 14 (1966), 302–307.
2. K.S. Kunz and J.L. Raymond, The finite-difference time-domain method for electromagnetics, CRC Press, Boca Raton, FL, 1993.
3. A. Taflove and S.C. Hagness, Computational electrodynamics. The finite-difference time-domain method, Artech House, Boston–London, 2000.
4. J. Fang, Time domain finite difference computation for Maxwell's equations, Ph.D. dissertation, EECS University of California, Berkeley, CA, 1989.
5. J.P. Berenger, Three-dimensional perfectly matched layer for the absorption of electromagnetic waves, J Computat Phys 127 (1996), 363–370.
6. J.L. Young, D. Gaitonde, and J.S. Shang, Toward the construction of a fourth-order difference scheme for transient EM wave simulation: Staggered cell approach, IEEE Trans Antennas Propagat 45 (1997), 1573–1580.
7. T. Hirono, W.W. Lui, S. Seki, and Y. Yoshikuni, A three dimensional fourth-order finite-difference time-domain scheme using a symplectic integrator propagator, IEEE Trans Microwave Theory Tech 49 (2001), 1640–1648.
8. T. Hirono, W.W. Lui, and K. Yokoyama, Time-domain simulation of electromagnetic field using a symplectic integrator, IEEE Microwave Guided Wave Lett 7 (1997), 279–281.
9. T. Hirono, W.W. Lui, K. Yokoyama, and S. Seki, Stability and dispersion of the symplectic fourth-order time-domain schemes for optical field simulation, Lightwave Technol 16 (1998), 1915–1920.
10. I. Saitoh, Y. Suzuki, and N. Takahashi, The symplectic finite difference time domain method, IEEE Trans Magn 37 (2001), 3251–3254.
11. I. Saitoh and N. Takahashi, Stability of symplectic finite-difference time-domain methods, IEEE Trans Magn 38 (2002), 665–668.
12. R. Rieben, D. White, and G. Rodrigue, High-order symplectic integration methods for finite element solutions to time dependent Maxwell equations, IEEE Trans Antennas Propagat 52 (2004), 2190–2195.
13. K. Mehmet, Y.O. Abdullah, and S.D. Daoub, Optimized exponential operator coefficients for symplectic FDTD method, IEEE Microwave Wireless Compon Lett 15 (2005), 86–88.

IN-LINE BEELINE CMRC AND APPLICATIONS TO COMPACT MICROSTRIP LOW-PASS FILTER

Fei Zhang,[1,2] Congying Gu,[3] Lina Shi,[1,2] Chengfang Li,[2] Jiangzhong Gu,[1] and Xiaowei Sun[1]
[1] Shanghai Institute of Microsystem and Information Technology
CAS
Shanghai, 200050, P. R. China
[2] Department of Physics
Wuhan University
Wuhan, 430072, P. R. China
[3] Department of Environmental Science and Engineering
Shanghai Jiaotong University
Shanghai, 200240, P. R. China

Received 28 November 2005

ABSTRACT: *A novel beeline compact microstrip resonant cell (BCMRC) is proposed in this paper. Its photonic bandgap and slow-wave effect are evaluated. The compact configuration presents superbroad stop-band and improved slow-wave characteristics. A low-pass filter, consisting of three BCMRCs connected in series, is designed and fabricated. The filter has the advantages of low insertion loss in the pass-band, sharp, high, and wide rejection in the stop-band, and compact size. Good agreement between the experimental and simulated results is achieved.* © 2006 Wiley Periodicals, Inc. Microwave Opt Technol Lett 48: 1125–1127, 2006; Published online in Wiley InterScience (www.interscience.wiley.com). DOI 10.1002/mop.21562

Key words: *compact microstrip resonant cell; photonic bandgap; low-pass filters; beeline circuits*

1. INTRODUCTION

Low-pass filters have been studied and exploited extensively as a key block in modern communication systems. Conventional microstrip low-pass filters (LPFs) have deep low- and high-impedance lines and serious discontinuities between them, or open stubs connected to junction elements. To remove these disadvantages, there has been much effort to develop a variety of compact microstrip low-pass filters using periodic structures such as photonic bandgap (BPG) and defected ground structure (DGS). Microstrip transmission lines incorporating a BPG or DGS structure exhibit bandstop and slow-wave characteristics, which can be exploited to reject unwanted frequency and to reduce the dimensions of the microstrip structure. One of the important properties of PBG and DGS is the increased slow-wave effect, which is caused by the equivalent inductance and capacitance. Hence, transmission